

Constraints on the fluctuation amplitude and density parameter from X-ray cluster number counts

Tetsu Kitayama¹ and Yasushi Suto^{1,2}

¹ Department of Physics, The University of Tokyo, Tokyo 113, Japan.

² Research Center For the Early Universe (RESCEU), School of Science,
The University of Tokyo, Tokyo 113, Japan.

e-mail: kitayama@utaphp2.phys.s.u-tokyo.ac.jp, suto@phys.s.u-tokyo.ac.jp

Received 1996 December 20; Accepted 1997 June 27

ABSTRACT

We find that the observed $\log N - \log S$ relation of X-ray clusters can be reproduced remarkably well with a certain range of values for the fluctuation amplitude σ_8 and the cosmological density parameter Ω_0 in cold dark matter (CDM) universes. The 1σ confidence limits on σ_8 in the CDM models with $n = 1$ and $h = 0.7$ are expressed as $(0.54 \pm 0.02)\Omega_0^{-0.35-0.82\Omega_0+0.55\Omega_0^2}$ ($\lambda_0 = 1 - \Omega_0$) and $(0.54 \pm 0.02)\Omega_0^{-0.28-0.91\Omega_0+0.68\Omega_0^2}$ ($\lambda_0 = 0$), where n is the primordial spectral index, and h and λ_0 are the dimensionless Hubble and cosmological constants. The errors quoted above indicate the statistical ones from the observed $\log N - \log S$ only, and the systematic uncertainty from our theoretical modelling of X-ray flux in the best-fit value of σ_8 is about 15%. In the case of $n = 1$, we find that the CDM models with $(\Omega_0, \lambda_0, h, \sigma_8) \simeq (0.3, 0.7, 0.7, 1)$ and $(0.45, 0, 0.7, 0.8)$ simultaneously account for the cluster $\log N - \log S$, X-ray temperature functions, and the normalization from the *COBE* 4 year data. The derived values assume the observations are without systematic errors, and we discuss in details other theoretical uncertainties which may change the limits on Ω_0 and σ_8 from the $\log N - \log S$ relation. We have shown the power of this new approach which will become a strong tool as the observations attain more precision.

Subject headings: cosmology: theory – dark matter – galaxies: clusters: general – X-rays: galaxies

Accepted for publication in The Astrophysical Journal.

1. Introduction

X-ray temperature and luminosity functions (hereafter XTF and XLF) of galaxy clusters provide important information on cosmology for various reasons; physics of the X-ray emission from clusters of galaxies is well understood, and a phenomenological model describing the temperature and density of intracluster gas, e.g., isothermal β -model, is reasonably successful. The dynamical time-scale of typical clusters is only an order of magnitude smaller than the age of the universe, but is much shorter than its cooling time-scale (except at the central core). This implies that such clusters retain the cosmological conditions at the epoch of their formation without being affected appreciably by the subsequent physical processes. Furthermore, one has a theoretical formalism to compute mass functions of virialized objects fairly reliably (Press & Schechter 1976, hereafter PS) which can be applied to predicting the XTF and XLF in a variety of cosmological models under reasonable assumptions of cluster evolution.

This methodology is particularly useful in estimating the amplitude of the density fluctuations. For instance, White, Efstathiou & Frenk (1993) found that σ_8 , the rms linear fluctuation in the mass distribution on a scale $8h^{-1}\text{Mpc}$ (h is the Hubble constant H_0 in units of $100 \text{ km s}^{-1} \text{ Mpc}^{-1}$), is approximately given by $\sigma_8 \sim 0.57\Omega_0^{-0.56}$ in the cold dark matter (CDM) models with $\lambda_0 = 1 - \Omega_0$, where Ω_0 is the density parameter and λ_0 is the dimensionless cosmological constant. More recently, several authors discussed the constraints on Ω_0 and λ_0 from the evolution of XTF and XLF (Kitayama & Suto 1996a,b, hereafter Papers I and II; Viana & Liddle 1996; Eke, Cole & Frenk 1996; Oukbir, Bartlett & Blanchard 1997).

The most commonly used XTF (Henry & Arnaud 1991) is, however, estimated from a small number of clusters ~ 20 , which ranges less than one order of magnitude in temperature, and hence the deduced constraints are statistically limited. On the contrary, the cluster number counts, $\log N$ - $\log S$, from recent observations (e.g., Rosati & Della Ceca 1997; Ebeling et al. 1997b) are constructed from a sample of hundreds of clusters and cover almost four orders of magnitude in flux. While Evrard & Henry (1991) and Blanchard et al. (1992) predicted the $\log N$ - $\log S$ of X-ray clusters, our present study compares the latest ROSAT observation with quantitative predictions in very specific cosmological models, and examines extensively several systematic uncertainties due to the theoretical modelling. Our main finding is that the latest $\log N$ - $\log S$ data can be reproduced well in CDM universes with a set of $(\Omega_0, \lambda_0, \sigma_8)$ which simultaneously account for the X-ray temperature functions, and the *COBE* 4 year data.

The anisotropies in the microwave background detected by *COBE* offer another independent way of estimating the fluctuation amplitude (e.g., Bunn & White 1997). The resulting estimate of σ_8 is, however, very sensitive to the value of the spectral index n of the primordial fluctuation spectrum as well as Ω_0 and λ_0 , because the scale probed by *COBE* ($\sim 1\text{Gpc}$) is about two orders of magnitude larger than $8h^{-1}\text{Mpc}$. On the other hand, σ_8 from the cluster abundance is fairly insensitive to the assumed value of n because clusters are more directly related to the density fluctuations around $10h^{-1}\text{Mpc}$. These two methods are, therefore, complementary in constraining cosmological models. In this paper, we adopt $n = 1$ for definiteness and derive limits on σ_8 and Ω_0 in $\lambda_0 = 1 - \Omega_0$ and $\lambda_0 = 0$ CDM universes from the cluster $\log N$ - $\log S$.

2. Theoretical prediction of the X-ray cluster number counts

We compute the number of clusters observed per unit solid angle with flux greater than S by

$$N(> S) = \int_0^\infty dz d_A^2(z) c \left| \frac{dt}{dz} \right| \int_S^\infty dS_0 (1+z)^3 n_M(M, z) \frac{dM}{dT} \frac{dT}{dL_{\text{band}}} \frac{dL_{\text{band}}}{dS_0}, \quad (1)$$

where c is the speed of light, t is the cosmic time, d_A is the angular diameter distance, T and L_{band} are respectively the temperature and the band-limited luminosity of clusters, and $n_M(M, z)dM$ is the comoving number density of virialized clusters of mass $M \sim M + dM$ at redshift z . To be strict, the redshift z at which one observes a cluster should be conceptually distinguished from its formation redshift z_f . There exist some formalisms to take account of the difference explicitly (e.g., Lacey & Cole 1993, hereafter LC; Papers I and II). In applying these formalisms, however, one needs an appropriate theory on the evolution of intracluster gas in each cluster between z_f and z , which is still highly uncertain and model-dependent at present. In the current analysis, therefore, we primarily use the standard PS theory to calculate $n_M(M, z)$ assuming $z_f = z$, and combine it with a phenomenological model of intracluster gas based upon the observed $L - T$ correlation. The effect of $z_f \neq z$ will be also discussed separately on the basis of the LC model following Paper II.

Given the observed flux S_0 and the redshift z of a cluster, we evaluate its luminosity L_{band} , temperature T , and mass M in the following manner. If the observed flux S_0 in equation (1) is given in a band $[E_a, E_b]$, the source luminosity L_{band} at z in the corresponding band $[E_a(1+z), E_b(1+z)]$ is written as

$$L_{\text{band}}[E_a(1+z), E_b(1+z)] = 4\pi d_L^2(z) S_0 [E_a, E_b], \quad (2)$$

where d_L is the luminosity distance. We then solve the following equations iteratively to obtain T :

$$L_{\text{bol}} = L_{44} \left(\frac{T}{6\text{keV}} \right)^\alpha (1+z)^\zeta 10^{44} h^{-2} \text{ erg sec}^{-1}, \quad (3)$$

$$L_{\text{band}}[T, E_a(1+z), E_b(1+z)] = L_{\text{bol}}(T) \times f[T, E_a(1+z), E_b(1+z)], \quad (4)$$

where $f[T, E_1, E_2]$ is the band correction factor to translate the bolometric luminosity $L_{\text{bol}}(T)$ into $L_{\text{band}}[T, E_1, E_2]$, and L_{44} , α and ζ are parameters which will be described shortly. In computing f , we take account of metal line emissions (Masai 1984) assuming the metallicity of 0.3 times the solar value, in addition to the thermal bremsstrahlung; the former makes significant contribution to the soft band luminosity especially at low temperature and is important for the present study where we use the ROSAT energy band, $E_a = 0.5\text{keV}$ and $E_b = 2.0\text{keV}$. Finally, assuming that the cluster gas is isothermal, we relate the temperature T to the mass M by

$$\begin{aligned} k_B T &= \gamma \frac{\mu m_p G M}{3 r_{\text{vir}}} \\ &= 5.2 \gamma \left(\frac{\Delta_{\text{vir}}}{18\pi^2} \right)^{1/3} \left(\frac{M}{10^{15} M_\odot} \right)^{2/3} (1+z_f) (\Omega_0 h^2)^{1/3} \text{ keV}, \end{aligned} \quad (5)$$

where γ is a parameter described later, k_B is the Boltzmann constant, G is the gravitational constant, m_p is the proton mass, and μ is the mean molecular weight (we adopt $\mu = 0.59$ throughout this paper). The virial radius $r_{\text{vir}}(M, z_f)$ is computed from Δ_{vir} , the ratio of the mean cluster density to the mean background density of the universe at z_f . We evaluate the latter using the formulae for the spherical collapse model presented in Paper II. The above methodology can be used to predict XTF and XLF as well. Except in considering the LC model discussed below, we set $z_f = z$ in the present analysis.

The above procedure has four parameters; L_{44} , α and ζ in the $L - T$ relation (3), and γ in the $T - M$ relation (5). For L_{44} and α , we adopt as our canonical choice $L_{44} = 2.9$ and $\alpha = 3.4$ from the observed present-day $L - T$ relation of David et al. (1993). We separately consider the cases of $L_{44} = 1.5$ and 5.5 , and $\alpha = 2.7$ and 4 in order to take account of the observed scatter to some extent. Figure 1 compares our model $L - T$ relation at $z = 0$ with recent observations; the data at higher temperatures ($T \gtrsim 1.5\text{keV}$) are of the X-ray brightest Abell-type clusters (XBACs; Ebeling et al. 1996) and the ones at lower temperatures ($T \lesssim 1\text{keV}$) are of Hickson’s compact groups (HCGs; Ponman et al. 1996). For both samples, we only plot the clusters with measured X-ray temperatures (73 clusters from XBACs and 16 from HCGs). For XBACs, we adopt the X-ray temperatures from the compilation of David et al. (1993) and convert the 0.1-2.4 keV band fluxes of Ebeling et al. (1996) to the bolometric luminosities using the Masai model (1984).

Figure 1 shows that our model $L - T$ relation (eq. [3] with $L_{44} = 2.9$ and $\alpha = 3.4$) is consistent with the observations of rich clusters and even small groups over almost two orders of magnitude in temperature. The best fit value for the slope α of the $L - T$ relation remains almost unchanged; $\alpha = 3.5$ from the XBACs sample only, and $\alpha = 3.3$ from combined samples of XBACs and HCGs. The range over which we vary L_{44} , $1.5 \sim 5.6$, corresponds to the $\pm 1\sigma$ scatter of the observed data when α is fixed to 3.4. Figure 1 also shows that varying α from 2.7 to 4.0 while fixing $L_{44} = 2.9$ roughly covers the scatter in the currently available $L - T$ data for the low temperature systems.

The parameter ζ specifies the redshift evolution of the $L - T$ relation. Since recent observations find little evidence for the evolution in the $L - T$ relation at $z \lesssim 0.4$ (e.g., Henry, Jiao & Gioia 1994; Mushotzky & Scarf 1997), we take $\zeta = 0$ (no evolution) as canonical, and also examine the cases of mild evolution $\zeta = -1$ and 1 to bracket the possible evolutionary effect.

The value of γ in the $T - M$ relation (5) would depend on the density profile of clusters as well as the ratio of galaxy kinetic energy to gas thermal energy. In fact, this parametrization with a single value of γ , common in the analysis with XTF, may be too simplified to represent the actual clusters of galaxies, but we also adopt this in this paper for simplicity. Previous authors mostly adopt values ranging from 1 to 1.5; $\gamma = 1$ (Papers I and II), $\gamma = 1.1$ (Viana & Liddle 1996), and $\gamma = 1.5$ (Eke et al. 1996). Recent observations seem to be roughly consistent with this range, though the scatter is admittedly large (Edge & Stewart 1991; Squires et al. 1996; Markevitch et al. 1996). Hereafter, unless otherwise stated, we adopt $\gamma = 1.2$ on the basis of the results of gas dynamical simulations by White et al. (1993), but again examine the cases of $\gamma = 1$ and 1.5 so as to see the systematic uncertainty due to this simplification.

For comparison, we also consider a theoretical $L - T$ relation based on the self-similar assumption (Kaiser 1986; Paper II). The thermal bremsstrahlung (free-free) component of the luminosity predicted in this model is

$$L_{\text{bol}}^{\text{ff}} = 1.2 \times 10^{45} \frac{A}{\gamma^{3/2}} \left(\frac{\Omega_{\text{B}}/\Omega_0}{0.1} \right)^2 \left(\frac{\Delta_{\text{vir}}}{18\pi^2} \right)^{1/2} \left(\frac{T}{6\text{keV}} \right)^2 (1 + z_f)^{3/2} (\Omega_0 h^2)^{1/2} \text{ erg sec}^{-1}, \quad (6)$$

where $\Omega_{\text{B}} = 0.0125h^{-2}$ is the baryon density parameter (e.g, Walker et al. 1991), and A is a fudge factor of order unity which depends on the specific density profile of intracluster gas. For the conventional β -model profile (eqs. [3.5]-[3.7] of Paper II), A is equal to 0.86 in the case of $(\Omega_0, \lambda_0, h) = (1, 0, 0.5)$, and 1.1 in the case of $(\Omega_0, \lambda_0, h) = (0.1, 0, 0.7)$. In practice, we also take account of metal line emissions (Masai 1984) in addition to the free-free component given above. Keeping in mind that the slope of the self-similar $L - T$ relation is apparently inconsistent with the observations as summarized in Figure 1, we simply intend to show the results of the simplest theoretical model. Figure 1 clearly exhibits that the amplitude of L in the self-similar model depends sensitively on the value of $\Omega_{\text{B}}/\Omega_0$, i.e., the gas mass fraction of the cluster. The

approach based on the observed $L - T$ relation (eq. [3]), on the contrary, is entirely independent of it.

In Figure 2, we plot our predictions of the cluster $\log N - \log S$ in various CDM models. We use the PS mass function in equation (1) and adopt our canonical set of parameters ($\alpha = 3.4$, $L_{44} = 2.9$, $\zeta = 0$, $\gamma = 1.2$) to evaluate the X-ray flux. We use our fitting formulae (Paper II) for the CDM mass fluctuation spectrum on the basis of Bardeen et al. (1996) transfer function. The observed data at fainter fluxes ($S < 10^{-12} \text{erg cm}^{-2} \text{s}^{-1}$) are taken from the *ROSAT* Deep Cluster Survey (RDCS, Rosati et al. 1995; Rosati & Della Ceca 1997) and those at brighter fluxes ($S > 10^{-12} \text{erg cm}^{-2} \text{s}^{-1}$) are from the *ROSAT* Brightest Cluster Sample (BCS, Ebeling et al. 1997a,b). In the analysis below, we use the RDCS data of Rosati & Della Ceca (1997) including the systematic errors according to Rosati (private communication) in addition to the statistical errors. The systematics come from the incompleteness in the optical identification of clusters at faint flux levels and from uncertainty in the flux determination on the basis of the wavelet analysis. The former would typically increase the upper error bar by +15% of $N(> S)$ at a given flux in the range of $2 \lesssim S \lesssim 3 \times 10^{-14} \text{erg cm}^{-2} \text{s}^{-1}$, while the latter would change S typically by +8% which is converted in the error of $N(> S)$. The error box for the BCS data is drawn from the best-fit power-law representation of the data (Ebeling, private communication). Since this error box simply represents the fitting errors, we assign the $\pm 1\sigma$ Poisson error (error bars at $S > 10^{-12} \text{erg cm}^{-2} \text{s}^{-1}$) estimated from the number of clusters in the BCS at a given S (the survey area of the BCS is 4.136 steradian). The Poisson error is used in the statistical analysis in §3.

Figure 2(a) displays the effect of different Ω_0 , λ_0 and h for $\sigma_8 = 1.04$ models, while Figure 2(b) shows that of different σ_8 in the cases of $\Omega = 1$ and 0.45. We find that the *COBE* normalized CDM models with $(\Omega_0, \lambda_0, h, \sigma_8) = (0.3, 0.7, 0.7, 1.04)$ and $(0.45, 0, 0.7, 0.83)$ reproduce remarkably well the observed $\log N - \log S$ over almost four orders of magnitude in flux provided that we adopt the canonical set of parameters. In the case of the standard CDM model with $(\Omega_0, \lambda_0, h) = (1, 0, 0.5)$, however, the *COBE* normalization ($\sigma_8 = 1.2$) significantly overproduces the number of clusters. This discrepancy becomes even worse for $h > 0.5$ where the *COBE* normalized σ_8 becomes larger. Therefore the standard CDM model is compatible with the cluster number counts only if $\sigma_8 = 0.56$, more than a factor of 2 smaller than the *COBE* normalization (standard CDM models with $n < 1$ can be consistent with both the *COBE* and $\log N - \log S$, but we do not explore the possibility in this paper). The predicted $\log N - \log S$ is sensitive to the values of Ω_0 and σ_8 , but rather insensitive to λ_0 and h .

Figure 3 exhibits how the predicted $\log N - \log S$ depends on different choices of parameters to model the $L - T$ and $T - M$ relations. We also plot the results based on the LC model, instead of the standard PS theory, in evaluating the mass function of virialized clusters. This model predicts the number of clusters of a given mass with explicitly taking account of their formation epochs z_f and the subsequent evolution. We assume that the temperature evolution of individual clusters is proportional to $[(1 + z_f)/(1 + z)]^s$ after z_f (see Paper II for details). Figures 3 (a) and 3 (b) indicate that varying α or ζ mainly changes the slope of the predicted $\log N - \log S$, while different values of L_{44} , γ or s affect the amplitude as well and may shift the $\log N - \log S$ predictions by a factor up to 5.

3. Constraints on Ω_0 and σ_8 in CDM models

Figure 4 summarizes the constraints on σ_8 and Ω_0 from cluster $\log N - \log S$, XTF and *COBE* 4 year results (Bunn & White 1997) in CDM universes with $h = 0.7$ and our standard cluster model ($\alpha = 3.4$, $L_{44} = 2.9$, $\zeta = 0$, $\gamma = 1.2$). We perform a χ^2 test of the $\log N - \log S$ using the six data points; at

$S[0.5-2.0 \text{ keV}] = 4 \times 10^{-14}$, 1.2×10^{-13} and $3 \times 10^{-13} \text{ erg cm}^{-2} \text{ s}^{-1}$ from RDCS (Rosati & Della Ceca 1997), 2×10^{-12} , 1×10^{-11} and $6 \times 10^{-11} \text{ erg cm}^{-2} \text{ s}^{-1}$ from BCS (Ebeling et al. 1997b) with appropriate statistical (and systematic) errors as discussed in the previous section. Strictly speaking, each data point of the cumulative number counts discussed here is not independent, but we treat all the above data points as independent. Since we have selected the six data points where the cluster numbers are different by a factor of $3 \sim 10$ from their neighboring points, we expect that this is not a bad approximation. In fact, we found that the constraint on Ω_0 and σ_8 plane is essentially determined by the two data points; at $2 \times 10^{-12} \text{ erg cm}^{-2} \text{ s}^{-1}$ from the BCS survey and at $4 \times 10^{-14} \text{ erg cm}^{-2} \text{ s}^{-1}$ from the RDCS. We would like to use the six data points because they would provide some additional information. Also we repeated the same analysis using twelve data points at different fluxes and made sure that the resulting constraints are insensitive to the choice. For comparison, we also perform a χ^2 test using the XTF data points and associated errors at $T = 3, 4.2, \text{ and } 6.2 \text{ keV}$ from Eke et al. (1996) who reanalysed the original data of Henry & Arnaud (1991).

Figure 4 indicates that constraints from the cluster $\log N$ - $\log S$ are consistent with, but stronger than, those from the XTF, because the observed $\log N$ - $\log S$ has smaller error bars than the XTF and covers wider dynamic range. Our 1σ (68%) confidence limits from cluster $\log N$ - $\log S$ are well fitted by

$$\sigma_8 = (0.54 \pm 0.02) \times \begin{cases} \Omega_0^{-0.35-0.82\Omega_0+0.55\Omega_0^2} & (\lambda_0 = 1 - \Omega_0), \\ \Omega_0^{-0.28-0.91\Omega_0+0.68\Omega_0^2} & (\lambda_0 = 0), \end{cases} \quad (7)$$

where the quoted errors include only the statistical ones due to the observed $\log N$ - $\log S$ relation (as will be discussed below, the systematic uncertainty of the above fit due to the theoretical modelling of cluster luminosity is estimated to be 15%). The *COBE* normalized $\Omega_0 = 1$ model is inconsistent with the cluster number counts at more than 3σ (99.7%) confidence. Observed cluster abundances and *COBE* normalization are simultaneously accounted for by the CDM model with $(\Omega_0, \lambda_0, \sigma_8) \simeq (0.3, 0.7, 1)$ and $(0.45, 0, 0.8)$ in the case of $h = 0.7$.

Figures 5 and 6 exhibit the systematic difference of the above results against our model assumptions in the $\lambda_0 = 1 - \Omega_0$ and $\lambda = 0$ models, respectively. These figures imply that the dependence of the $\Omega_0 - \sigma_8$ constraints on our model parameters are very similar in $\lambda_0 = 1 - \Omega_0$ and $\lambda = 0$ models. Panels (a) indicate that varying L_{44} from our canonical value 2.9 to 1.5 (5.5) will systematically increase (decrease) the best-fit σ_8 value for a given Ω_0 by about 15%. The range of L_{44} considered here roughly corresponds to the $\pm 1\sigma$ scatter in the observed $L - T$ relation (see also Fig.1). Although this scatter may be partly due to the observational uncertainties in determining the temperature, we conservatively interpret it as an intrinsic scatter in the $L - T$ relation which results in the systematic error for the best-fit σ_8 value by 15%.

Panels (b) to (e) of Figures 5 and 6 show the systematic effects due to the other model parameters. The best-fit $\Omega_0 - \sigma_8$ relation (eq. [7]) is shown to be rather robust against α and ζ over the ranges considered here; the changes in these parameters merely move the contours along the best-fit relation. This is because α and ζ mainly affect the slope of the predicted $\log N$ - $\log S$ (Fig.3) and such changes are compensated by altering the CDM fluctuation spectrum with Ω_0 and σ_8 . On the other hand, allowing for the changes of $1 < \gamma < 1.5$ and $0 < s < 1$, the best-fit σ_8 value shifts in a comparable amount to that due to the changes of $1.5 < L_{44} < 5.5$. Note that the changes in γ and s change the XTF and $\log N$ - $\log S$ contours in a similar manner, and the resulting constraints from the $\log N$ - $\log S$ and XTF remain consistent with each other.

The ranges of parameters α , ζ , γ and s considered in Figures 5 and 6 are, unlike that of L_{44} , not directly related to definite statistical consideration. Furthermore, it is difficult to judge quantitatively how their intrinsic uncertainties correlate with one another. So we simply illustrate their individual effects in the figures, and quote only the representative systematic error due to L_{44} for definiteness and simplicity.

As is clear from Figures 5 and 6, with the ranges of the parameters considered here, the error due to L_{44} represents a reasonable estimate for the total systematic uncertainty in the best-fit σ_8 value.

Panels (f) of Figures 5 and 6 show that the cluster number counts is very insensitive to h unlike the *COBE* normalization. The best-fit cosmological parameters for both the *COBE* data and the cluster abundance are $(\Omega_0, \lambda_0, \sigma_8) \simeq (0.25, 0.75, 1.1), (0.4, 0, 0.9)$ in the case of $h = 0.8$, and $(0.5, 0.5, 0.8), (0.6, 0, 0.75)$ in the case of $h = 0.5$.

Another interesting application of X-ray cluster number counts can be found in probing the underlying $L - T$ relation. Figures 4, 5 and 6 indicate that the $\log N - \log S$ and XTF contours overlap with each other at the $\pm 1\sigma$ level for our canonical $L - T$ relation with $2.7 < \alpha < 4$ or $-1 < \zeta < 1$. On the other hand, $\log N - \log S$ and the XLF constraint is in good agreement with each other only with $L_{44} = 2.9$; $L_{44} = 1.5$ or 5.5 is marginally consistent with the XTF constraint at the 2σ level. Incidentally if we use the theoretical $L - T$ relation briefly described in the previous section, the $\log N - \log S$ and XTF contours do not agree with each other even at the 3σ level. These reflect the fact that the predicted $\log N - \log S$ is sensitive to the adopted $L - T$ relation (Fig. 3). Thus, with more accurate determination of the $\log N - \log S$ and XTF by the future observations, one will be able to constrain the $L - T$ relation more tightly.

4. Conclusions

We have found that there is a set of theoretical models which successfully reproduce the observed $\log N - \log S$ relation of galaxy clusters over almost four orders of magnitude in the X-ray flux. This is by no means a trivial result itself, and more interestingly low density CDM models with $(\Omega_0, \lambda_0, h, \sigma_8) \simeq (0.3, 0.7, 0.7, 1)$ and $(0.45, 0, 0.7, 0.8)$ in particular simultaneously account for the cluster $\log N - \log S$, XTF, and the *COBE* 4 year results. Constraints on the density fluctuation spectrum from the abundance of galaxy clusters are in fact complementary to those from other observations, such as the cosmic microwave background radiation (Bunn & White 1997) and the galaxy correlation functions (Peacock 1997). Our $\log N - \log S$ results confirm that the *COBE* normalized CDM models with $\Omega_0 = 1$ and $h \gtrsim 0.5$ cannot account for the cluster abundances. The derived values assume the observations are without systematic errors, and we discuss in details other theoretical uncertainties which may change the limits on Ω_0 and σ_8 from the $\log N - \log S$ relation. Incidentally these conclusions are also in good agreement with the recent finding of Shimasaku (1997) on the basis of the X-ray cluster gas mass function and the big-bang nucleosynthesis consideration.

Although we have mainly considered CDM models with $n = 1$ and $h = 0.7$, our procedure can be easily extended to other cosmological models. The observed $\log N - \log S$ data with better statistical significance can put more stringent limits on the parameters than the previous estimates based on the XTF and XLF. Since the $\log N - \log S$ at low fluxes is sensitive to the underlying $L - T$ relation, one may probe this relation using the improved data of the $\log N - \log S$ and XTF which will become available in the near future. In summary, we have shown the power of this new approach which will become a strong tool as the observations attain more precision.

We deeply thank Piero Rosati, Harald Ebeling, and Patrick Henry for kindly providing us with the X-ray data prior to their publication. We also thank Shin Sasaki for stimulating discussion, and an anonymous referee for useful comments which helped improve the paper. T.K. acknowledges support from a JSPS (Japan Society of Promotion of Science) fellowship. This research was supported in part by the

Grants-in-Aid by the Ministry of Education, Science, Sports and Culture of Japan (07CE2002) to RESCEU (Research Center for the Early Universe).

Note Added: After we submitted this paper, Mathiesen & Evrard posted a preprint (astro-ph/9703176) which also demonstrated the potential importance of the $\log N$ - $\log S$ relation, combined with the temperature-luminosity relation, for constraining cosmological parameters. Their results are basically consistent with what we found.

REFERENCES

- Bardeen, J. M., Bond, J. R., Kaiser, N. & Szalay, A. S. 1986, ApJ, 304, 15
- Blanchard, A., Wachter, K., Evrard, A. E., & Silk, J. 1992, ApJ, 391, 1
- Bunn, E. F., & White, M. 1997, ApJ, 480, 6
- David, L. P., Slyz, A., Jones, C., Forman, W., & Vrtilik, S. D. 1993, ApJ, 412, 479
- Ebeling, H., Voges, W., Böhringer, H., Edge, A. C., Huchra, J. P., & Briel, U. G. 1996, MNRAS, 281, 799
- Ebeling, H., Edge, A. C., Fabian, A. C., Allen, S. W., & Crawford C. S. 1997a, ApJ, 479, L101
- Ebeling H., et al. 1997b, MNRAS, submitted.
- Edge, A. C., & Stewart, G. C. 1991, MNRAS, 252, 428
- Eke, V. R., Cole, S., & Frenk, C. S. 1996, MNRAS, 282, 263
- Evrard, A. E., & Henry, J. P. 1991, ApJ, 383, 95
- Henry, J. P., & Arnaud, K. A. 1991, ApJ, 372, 410
- Henry, J. P., Jiao, L., & Gioia, I. M. 1994, ApJ, 432, 49
- Kitayama, T., & Suto, Y. 1996a, MNRAS, 280, 638 (Paper I)
- Kitayama, T., & Suto, Y. 1996b, ApJ, 469, 480 (Paper II)
- Lacey, C. G., & Cole, S. 1993, MNRAS, 262, 627 (LC)
- Markevitch, M., Mushotzky, R., Inoue, H., Yamashita, K., Furuzawa, A., & Tawara, Y. 1996, ApJ, 456, 437
- Masai, K. 1984, Ap&SS, 98, 367
- Mathiesen, B. & Evrard, A. E. 1997, MNRAS, submitted (astro-ph/9703176).
- Mushotzky, R.F., & Scharf, C. A. 1997, ApJ, 482, L13
- Oukbir, J., Bartlett, J. G., & Blanchard, A. 1997, A&A, 320, 3650
- Peacock, J. A. 1997, MNRAS, 284, 885
- Ponman, T. J., Bourner, P. D. J., Ebeling, H., & Böhringer, H. 1996, MNRAS, 283, 690
- Press, W. H., & Schechter, P. 1974, ApJ, 187, 425 (PS)
- Rosati, P., Della Ceca, R., Burg R., Norman, C., & Giacconi, R. 1995, ApJ, 445, L11
- Rosati, P., & Della Ceca, R. 1997, in preparation.
- Shimasaku, K. 1997, submitted to ApJ.
- Squires, G., Kaiser, N., Babul, A., Fahlman, G., Woods, D., Neumann, D.M., Böhringer, H. 1996, ApJ, 461, 572
- Viana, P. T. P., & Liddle, A. R. 1996, MNRAS, 281, 323
- Walker T. P., Steigman G., Schramm D. N., Olive K. A., & Kang H. -S. 1991, ApJ, 376, 51
- White, S. D. M., Efstathiou, G., & Frenk, C. S. 1993, MNRAS, 262, 1023
- White, S. D. M., Navarro, J. F., Evrard, A. E., & Frenk, C. S. 1993, Nature, 366, 429

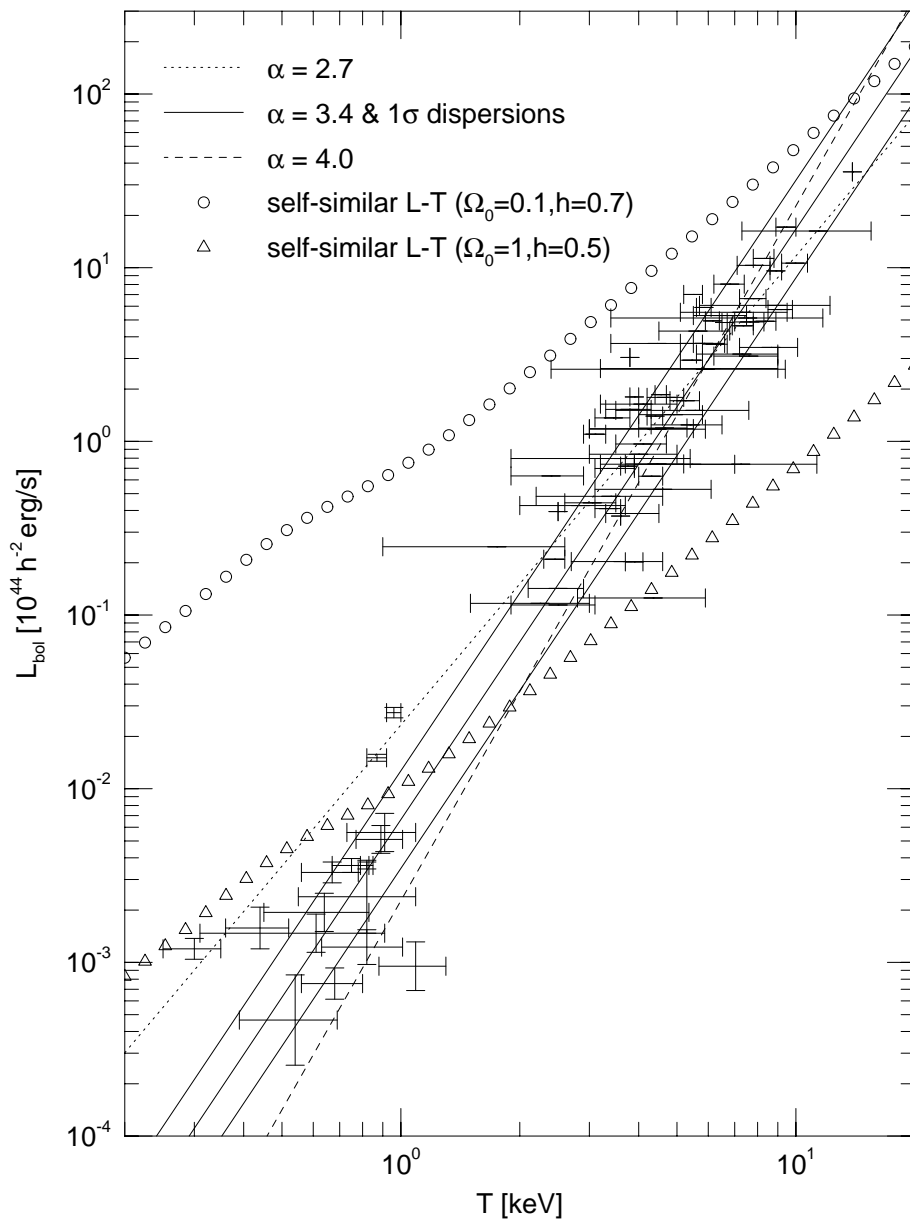


Fig. 1.— The $L - T$ relation of X-ray clusters (at $z = 0$). The data points at $T \gtrsim 1.5 \text{ keV}$ are from X-ray brightest Abell-type clusters (XBACs, Ebeling et al. 1996) while those at $T \lesssim 1 \text{ keV}$ are from Hickson's compact groups (HCGs, Ponman et al. 1996). Solid lines show our canonical $L - T$ relation (3) with $L_{44} = 2.9$ and $\alpha = 3.4$ (David et al. 1993) and its 1σ scatter computed from the data points. Dotted line shows the $L - T$ relation with $L_{44} = 2.9$ and $\alpha = 2.7$, and the dashed line with $L_{44} = 2.9$ and $\alpha = 4$. Also plotted are the theoretical $L - T$ relations based on the self-similar assumption for $(\Omega_0, \lambda_0, h) = (1, 0, 0.5)$ (open triangles) and $(0.1, 0, 0.7)$ (open circles).

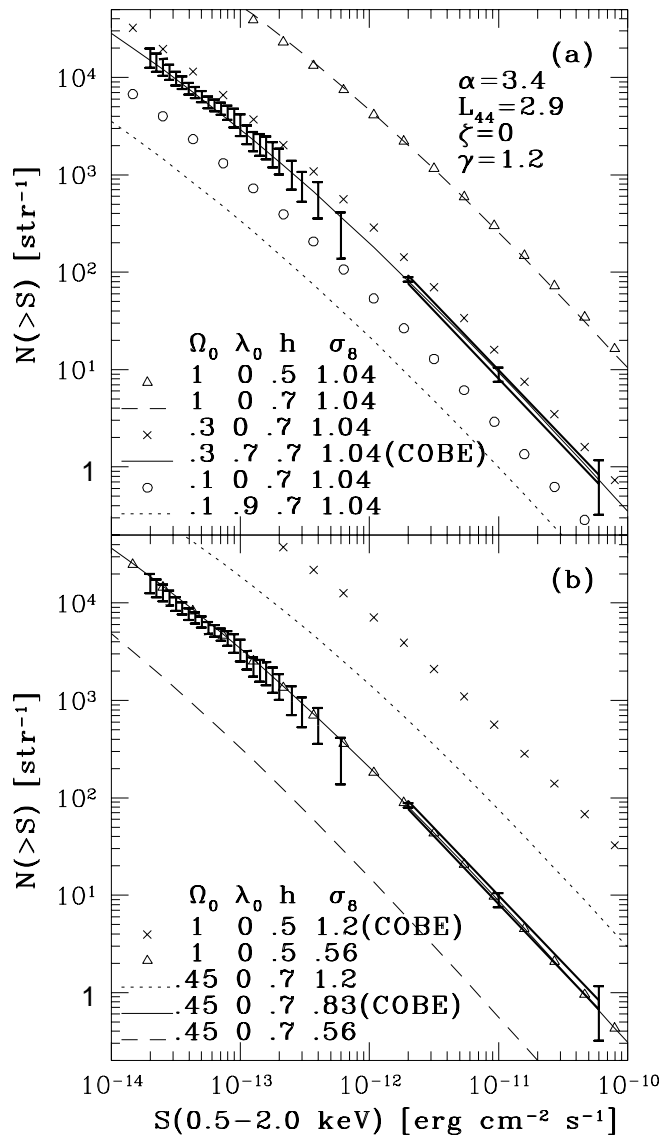


Fig. 2.— Theoretical predictions for $\log N$ - $\log S$ of X-ray clusters in CDM models with different cosmological parameters; (a) $\sigma_8 = 1.04$ models with different Ω_0 , λ_0 and h , (b) $\Omega_0 = 1$ and 0.45 models with different σ_8 . Denoted by (COBE) are the models normalized according to the *COBE* 4 year data (Bunn & White 1997). Data points with error bars at $S \lesssim 10^{-12}$ erg cm⁻² s⁻¹ are from the *ROSAT* Deep Cluster Survey (RDCS, Rosati et al. 1995; Rosati & Della Ceca 1997), and the error box at $S \gtrsim 2 \times 10^{-12}$ represents a power-law fitted region from the *ROSAT* Brightest Cluster Sample (BCS, Ebeling et al. 1997a,b). For the BCS data at $S = 2 \times 10^{-12}$, 1×10^{-11} and 6×10^{-11} erg cm⁻² s⁻¹, we also plot the corresponding Poisson errors.

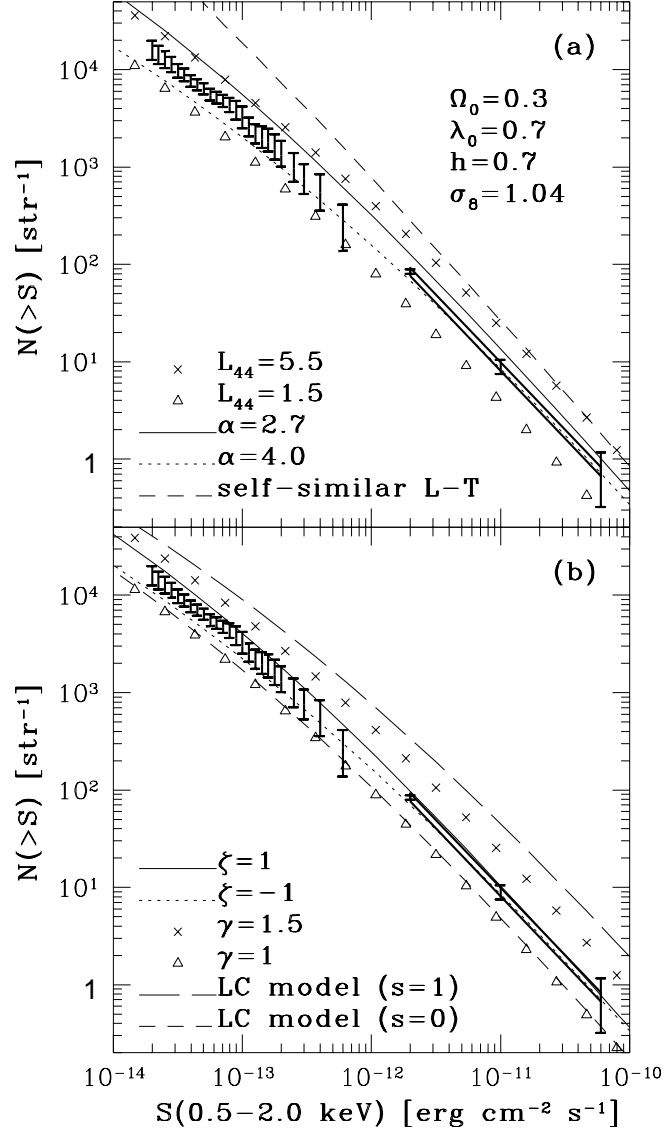


Fig. 3.— Theoretical predictions for $\log N$ - $\log S$ of X-ray clusters in a CDM model ($\Omega_0 = 0.3$, $\lambda_0 = 0.7$, $h = 0.7$, $\sigma_8 = 1.04$); (a) with different L_{44} and α as well as the theoretical $L - T$ relation based on the self-similar assumption, (b) with different ζ and γ as well as the LC model characterised by $T(z) \propto [(1 + z_f)/(1 + z)]^s$ (see main text).

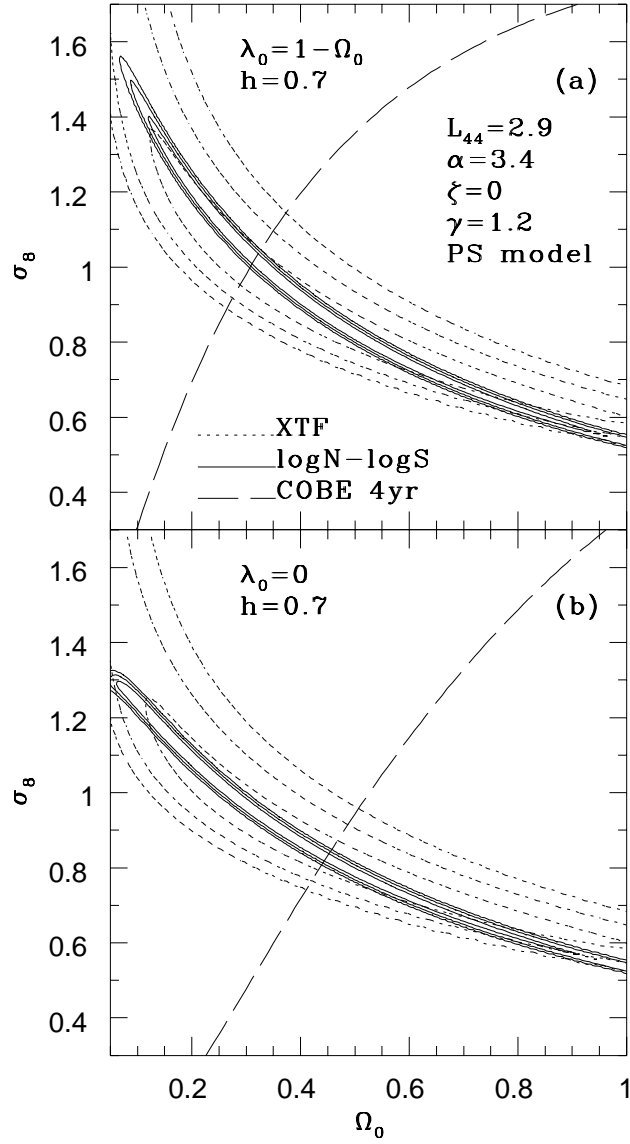


Fig. 4.— Limits on Ω_0 and σ_8 in CDM models ($n = 1$, $h = 0.7$) with (a) $\lambda_0 = 1 - \Omega_0$, and (b) $\lambda_0 = 0$. Constraints from cluster $\log N - \log S$ (solid) and XTF (dotted) are plotted as contours at 1σ (68%), 2σ (95%) and 3σ (99.7%) confidence levels. Dashed lines indicate the *COBE* 4 year results from Bunn & White (1997).

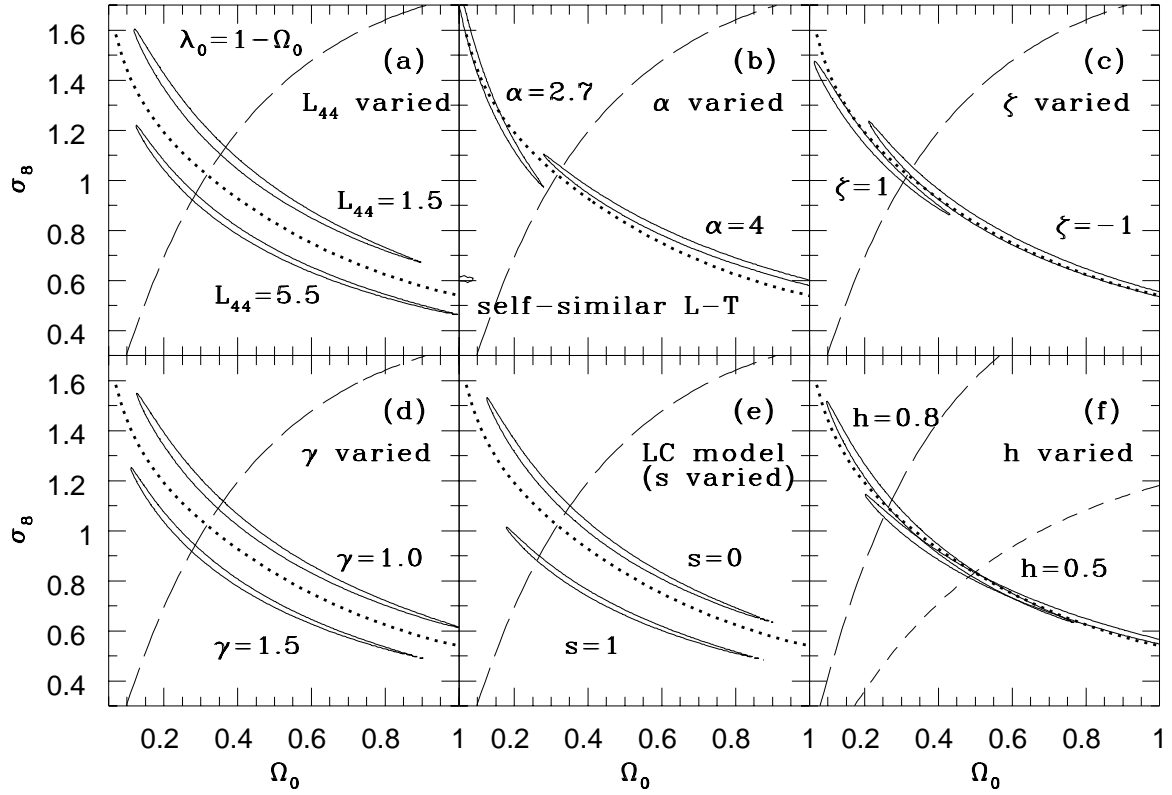


Fig. 5.— Systematic effects on the $\Omega_0 - \sigma_8$ constraints in $\lambda_0 = 1 - \Omega_0$ CDM models. The $1\sigma(68\%)$ confidence contours from the cluster $\log N - \log S$ are plotted for different (a) L_{44} , (b) α , (c) ζ , (d) γ , (e) s , and (f) h . Except for the parameters varied in each panel, our canonical set of parameters ($L_{44} = 2.9$, $\alpha = 3.4$, $\zeta = 0$, $\gamma = 1.2$, $h = 0.7$) and the PS model are used. Dotted and dashed lines represent our best-fit for the canonical parameter set (eq. [7]) and the *COBE* 4 year results, respectively.

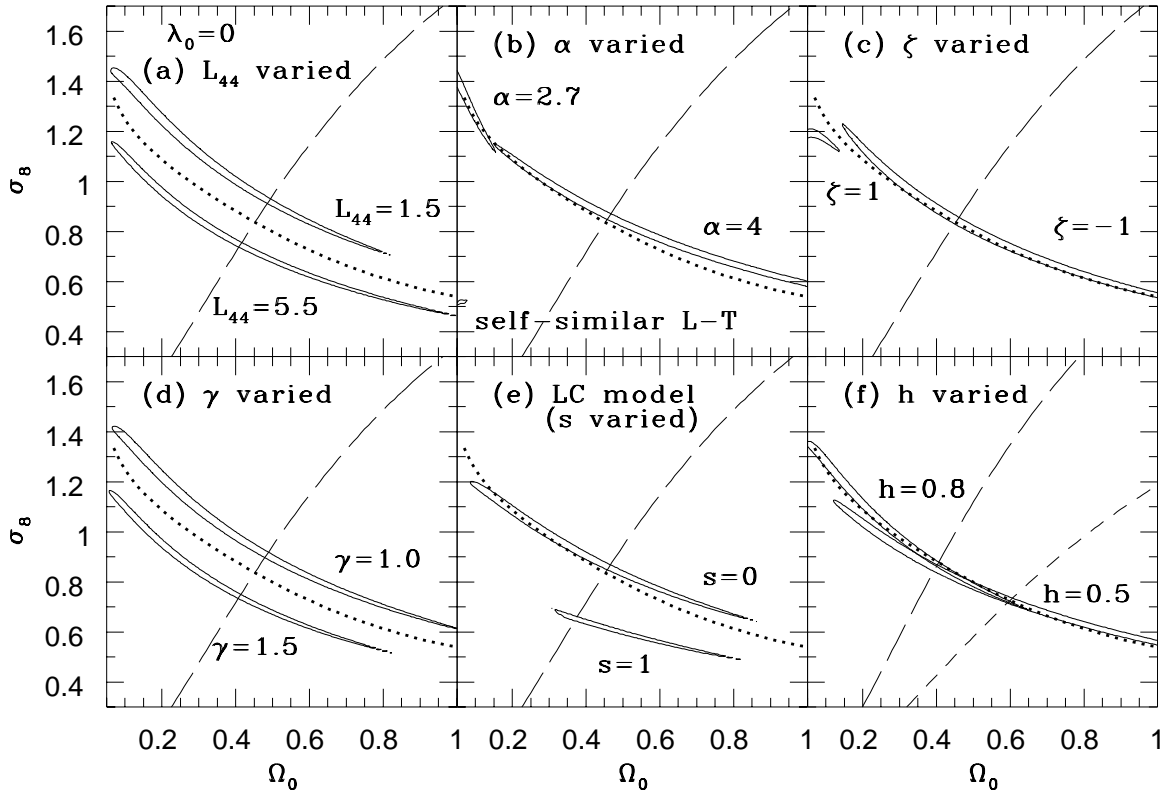


Fig. 6.— Same as Figure 5, but for $\lambda_0 = 0$ CDM models.